



Cite this: DOI: 10.1039/d5tc03382a

## Preferentially oriented $\text{SrTiO}_3$ thin films grown on lanthanide-assisted $\text{Si}(001)$ via pulsed laser deposition

Hannes Rijckaert, <sup>a</sup> Giovanna Latronico, <sup>b</sup> Davy Deduytsche, <sup>c</sup> Eduardo Solano, <sup>d</sup> Petriina Paturi <sup>e</sup> and Paolo Mele <sup>f</sup>

The integration of high-quality  $\text{SrTiO}_3$  thin films on silicon substrates is crucial for various applications. This work investigates the use of an out-of-plane, self-oriented  $\text{La}_2\text{O}_2\text{CO}_3$  seed layer prepared via the chemical solution deposition (CSD) method as a template for  $\text{SrTiO}_3$  growth by pulsed laser deposition (PLD). The growth window of the  $\text{SrTiO}_3$  thin film was determined by *in situ* X-ray diffraction and by studying the thermal stability of the  $\text{La}_2\text{O}_2\text{CO}_3$  film. This study resulted in crack-free films with preferential but not exclusive  $(001)$  out-of-plane orientation when using one-step PLD deposition at 750 °C. Further in-depth X-ray diffraction analysis revealed that the  $\text{SrTiO}_3$  film exhibited multiple preferential orientations rather than a continuous fibre texture. Transmission electron microscopy confirmed a uniform  $\text{SrTiO}_3$  film without interfacial reactions and a homogeneous composition. These findings highlight the key role of deposition conditions in controlling crystallinity and orientation, enabling the integration of high-quality perovskite oxide on silicon.

Received 10th September 2025,  
Accepted 10th December 2025

DOI: 10.1039/d5tc03382a

rsc.li/materials-c

## Introduction

Recently, strontium titanate ( $\text{SrTiO}_3$ ) thin films have emerged as a promising lead-free material due to their functional and practical advantages. In terms of functional properties,  $\text{SrTiO}_3$  exhibits a large dielectric constant, high breakdown strength, and tunable electrical conductivity *via* doping. These properties make it attractive for applications in energy storage and non-volatile memory devices.<sup>1,2</sup> Additionally,  $\text{SrTiO}_3$  is identified as an ideal candidate for cryogenic applications due to its low Curie temperature, enabling the exploration of piezo-electric and electro-optic effects at cryogenic temperatures.<sup>3</sup> Room-temperature

ferroelectric properties, such as the electrocaloric effect, have also been reported when epitaxial strain is achieved *via* strain engineering due to the lattice mismatch with appropriate substrates.<sup>4,5</sup>

In fact, beyond their potential use with functionality in several applications, these  $\text{SrTiO}_3$  thin films can serve effectively as buffer template layers for the monolithic integration of Ge, III-V heterostructures, or other perovskite oxide materials such as  $\text{BaTiO}_3$ ,  $\text{SrRuO}_3$  and  $\text{Pb}(\text{Zr}, \text{Ti})\text{O}_3$  (PZT) on  $\text{Si}(001)$  wafers.<sup>6-8</sup> Therefore, the direct heteroepitaxy of  $\text{SrTiO}_3$  on Si wafers is an important step toward enabling the integration of multifunctional perovskite oxides onto large-scale wafers. Several deposition techniques have been introduced to grow  $\text{SrTiO}_3$  thin films as a buffer layer on Si wafers, with molecular-beam epitaxy (MBE) and pulsed laser deposition (PLD) being two of the most commonly used methods.<sup>9</sup>

MBE is suitable for epitaxial growth due to its slow growth rate and precise control of atomic growth. However, the low oxygen partial pressure, typically limited to a maximum of  $10^{-5}$  mbar, promotes the formation of oxygen vacancies in the  $\text{SrTiO}_3$  thin film, which significantly influences functional properties.<sup>10</sup> To eliminate these oxygen vacancies, post-annealing at high temperatures, especially under high oxygen pressure, is introduced, resulting in generally strong interfacial reactions with Si substrates.<sup>10</sup> Compared to the MBE technique, PLD can reach a higher oxygen pressure of above  $10^{-2}$  mbar and offers better control over oxygen vacancies. Nevertheless,

<sup>a</sup> SCriPTS, Department of Chemistry, Ghent University, Krijgslaan 281-S3, 9000 Ghent, Belgium. E-mail: Hannes.Rijckaert@UGent.be

<sup>b</sup> Shibaura Research Laboratories, Shibaura Institute of Technology, Omiya Campus, 307 Fukasaku, Minuma-ku, Saitama City, Saitama 337-8570, Japan

<sup>c</sup> CoCooN Group, Department of Solid State Sciences, Ghent University, Krijgslaan 281-S1, 9000 Ghent, Belgium

<sup>d</sup> NCD-SWEET beamline, ALBA Synchrotron Light Source, Carrer de la Llum 2-26, 08290 Cerdanyola del Vallès, Spain

<sup>e</sup> Wihuri Physical Laboratory, Department of Physics and Astronomy, University of Turku, Vesilinnantie 5, 20014, Turku, Finland

<sup>f</sup> College of Engineering, Shibaura Institute of Technology, Omiya Campus, 307 Fukasaku, Minuma-ku, Saitama City, Saitama 337-8570, Japan

† These authors contributed equally to this work.

‡ Present address: Institute of Condensed Matter Chemistry and Technologies for Energy, National Research Council of Italy (ICMATE-CNR), Via Gaetano Previati 1/E, 23900 Lecco, Italy.



the direct epitaxy of oxides on the Si wafer by PLD is still a challenge due to the higher O<sub>2</sub> pressure, which results in amorphous SiO<sub>2</sub> interface formation and a lack of atomic control. This shows the difficulty of growing various multi-functional perovskite oxide materials on Si wafers due to the presence of the interfacial SiO<sub>2</sub> layer, which prevents direct oriented growth. Prior to the direct deposition onto Si wafers, this interfacial oxide needs to be properly addressed.

Several approaches reported in the literature have been proposed to overcome this issue. A commonly used method involves introducing a SrO buffer layer,<sup>11</sup> although this often leads to SrTiO<sub>3</sub> thin-film growth in the (110) orientation, which may not be desirable for all applications. Another strategy is the thermal treatment of the Si wafer by heating it to approximately 980 °C in an ultra-high vacuum to remove the native oxide.<sup>12–14</sup> Alternatively, chemical etching with a 1% HF solution can be used to produce a hydrogen-terminated Si surface,<sup>11</sup> which is preferred for pure oxide growth. A two-step deposition method has also been reported, where a thin SrTiO<sub>3</sub> layer is first deposited at low temperature between 150 and 300 °C in a vacuum to initiate nucleation, followed by a final deposition step at 650 °C to enhance crystallinity and film quality.<sup>11,15</sup> The group at the University of Twente<sup>16,17</sup> has introduced inorganic 2D Ca<sub>2</sub>Nb<sub>3</sub>O<sub>10</sub> nanosheets as a growth template layer on the Si wafer to grow artificial heteroepitaxial SrTiO<sub>3</sub> thin films with (001) orientation.

Building on all these methods and addressing the challenges of large-area, wafer-scale deposition with high-throughput *via* PLD and MBE,<sup>18</sup> we present a promising, high-throughput chemical solution deposition (CSD) process that uses a self-oriented La<sub>2</sub>O<sub>2</sub>CO<sub>3</sub> template film, based on the work of Picavet *et al.*,<sup>19</sup> to grow well-oriented SrTiO<sub>3</sub> thin films on Si wafers using the PLD technique. The resulting highly textured film exhibits a preferential out-of-plane orientation and can serve as an integration tool for the growth of multi-functional perovskite oxide materials on Si-based platforms where full epitaxy is not required. Thus, the key factor is achieving a crystalline, textured, and preferentially oriented film that exhibits the desired ferroelectric and dielectric properties.

## Experimental section

STO thin films were deposited on both La<sub>2</sub>O<sub>2</sub>CO<sub>3</sub>-templated and pristine Si(001) substrates using PLD. The Si substrates were cleaned by ultrasonic treatment in isopropanol (Kanto Chemical, >99.7%) for 5 minutes, followed by heating on a hotplate at 150 °C under ambient conditions to remove any solvent residues. The formulation of the precursor solution and the CSD method for growing the La<sub>2</sub>O<sub>2</sub>CO<sub>3</sub> template film have been reported in previous works.<sup>19,20</sup> A polyvinylpyrrolidone (PVP)-based solution was prepared by dissolving 0.05 g of a 40 wt% PVP solution (Alfa Aesar, 8000 g mol<sup>-1</sup>) in H<sub>2</sub>O into 40 mL of n-propanol (Chem-Lab, 99.8%). The La<sub>2</sub>O<sub>2</sub>CO<sub>3</sub> solution was prepared by dissolving La(NO<sub>3</sub>)<sub>3</sub>·6H<sub>2</sub>O (Merck,

≥99.99%) in n-propanol with a concentration of 0.06 mol L<sup>-1</sup>. The PVP solution was spin-coated onto treated 10 × 10 mm<sup>2</sup> Si substrates at a spin rate of 2600 rpm for 30 seconds using the Kyowariken K-359S1 spin coater to enhance the wetting behavior at the surface interface. Directly after this spin-coating, the La<sub>2</sub>O<sub>2</sub>CO<sub>3</sub> solution was spin-coated onto the PVP-modified Si substrate using the same spin-coating parameters. Subsequently, the coated substrates underwent a pyrolysis step at 200 °C for 5 minutes in ambient air, followed by an annealing step in dry static air with a heating rate of 12.5 °C min<sup>-1</sup> to a final temperature of 485 °C, and were held for a dwelling time of 20 minutes. A stoichiometric SrTiO<sub>3</sub> target (Toshima, purity 99.99%) was used for PLD growth with a Nd:YAG laser (YG-PLAD-241, LOTIS-TII, Minsk, Belarus) at a wavelength of 266 nm (fourth harmonic). The optimized laser parameters for high-quality SrTiO<sub>3</sub> thin films were a repetition rate of 10 Hz and a laser fluence of 4 J cm<sup>-2</sup>. The distance between the target and the substrate was maintained at 35 mm.

For determining deposition and growth windows, thermogravimetric analysis (TGA) and differential thermal analysis (DTA) were used with a NETZSCH (Selb, Germany) Model STA 449F3 Jupiter system at a heating rate of 10 °C min<sup>-1</sup> under air atmosphere to understand the thermal decomposition of the La<sub>2</sub>O<sub>2</sub>CO<sub>3</sub> precursor as a function of temperature. *In situ* X-ray diffraction (XRD) scans were carried out on a Bruker D8 Discover diffractometer equipped with a home-built annealing chamber (Ghent University) and a linear detector. Cu K $\alpha$  radiation ( $\lambda = 1.5406 \text{ \AA}$ ) was employed, and the sample was annealed in ambient air at a heating rate of 5 °C min<sup>-1</sup> up to 750 °C, with data collected in the 2 $\theta$  range of 20° to 50° and an integration time of 15 s. Before and after the annealing, *ex situ* XRD scans from 15° to 60° with a step size of 0.05° and an integration time of 1 s were taken. Atomic force microscopy measurements were carried out using a Bruker ICON Dimension microscope operated on tapping mode in air with Bruker TESPA-V2 cantilevers.

All the thin films were analyzed *via* *ex situ* XRD after the PLD depositions. Data acquisition was performed using a Bragg-Brentano powder diffractometer (Smart Lab Rigaku Corporation, Japan) with Cu K $\alpha$  radiation ( $\lambda = 1.5406 \text{ \AA}$ ) over an angular range of 15°–55° with an angular step of 0.01° (power settings: 50 mA, 40 kV). The grazing-incidence wide-angle X-ray scattering (GIWAXS) data were collected at the NCD-SWEET beamline of the ALBA Synchrotron Radiation Facility (Spain). The incident X-ray beam energy was set to 12.4 keV ( $\lambda = 0.9998 \text{ \AA}$ ) using a channel-cut Si(111) monochromator. A stack of Be compound refractive lenses was employed to collimate the beam, resulting in a beam size of 50 × 150  $\mu\text{m}^2$  ( $V \times H$ ) at the sample position. The angle of incidence ( $\alpha_i$ ) was screened between 0° and 1°, and finally set to 0.325° to ensure surface sensitivity. An exposure time of 10 s was used. The scattering patterns were recorded using a Rayonix LX255-HS area detector, which consists of 1920 × 5760 pixels ( $H \times V$ ) with a pixel size of 44.27 × 44.27  $\mu\text{m}^2$ . The scattering vector  $q$  was calibrated using Cr<sub>2</sub>O<sub>3</sub> as a standard, resulting in a sample-to-detector distance of 201.65 mm. The pole figures were measured using a Panalytical Empyrean



diffractometer with a 5-axis goniometer, a Bragg-Brentano<sup>HD</sup> collimator and a PIXcel3D detector using Cu K $\alpha$  radiation. The pole figures were measured at constant  $2\theta/\omega$  angles by varying the tilt angle ( $\chi$ ) and rotation angle ( $\phi$ ) and using the receiving slit mode with 0.25° width.

The topographical properties were characterized using scanning electron microscopy (SEM) with an FEI Nova 600 Nanolab Dual Beam system. Transmission electron microscopy (TEM) was used to study the microstructural properties of SrTiO<sub>3</sub> films with a bright field (BF) detector and operated at a JEOL JEM-2200FS of the UGent TEM core facility with a working voltage of 200 kV. The composition was determined *via* energy-dispersive X-ray (EDX) spectroscopy and high-angle annular dark-field (HAADF) imaging in scanning TEM (STEM). For TEM investigations, a cross-sectional lamella was prepared by focused ion beam, utilizing an FEI Nova 600 dual beam system, following the procedure described in this technical note.<sup>21</sup>

## Results and discussion

The out-of-plane self-oriented La<sub>2</sub>O<sub>2</sub>CO<sub>3</sub> seed layer has been extensively described in the work of Picavet *et al.*,<sup>19</sup> demonstrating its potential as a general integration tool for various ferroelectric films deposited *via* the CSD approach. This La<sub>2</sub>O<sub>2</sub>CO<sub>3</sub> film exhibits a monoclinic structure (Type 1a) and has an in-plane lattice spacing (a) of 4.076 Å. Seed layers are required to act as a texture template for growth; their effectiveness is limited by the lattice spacing and the occupation of sites within the crystal lattice. Therefore, the lattice mismatch between the seed and the functional layer should be minimized as much as possible to grow a high-quality layer. Cubic SrTiO<sub>3</sub> (space group: *Pm*<sub>3</sub>*m*, 221, PDF: 00-035-0734), with a bulk in-plane lattice spacing (a) of 3.905 Å, results in a theoretical tensile lattice mismatch of +4.2%, indicating the possibility of forming a tensile-strained SrTiO<sub>3</sub> film. Therefore, La<sub>2</sub>O<sub>2</sub>CO<sub>3</sub> film appears to be a promising candidate for growing SrTiO<sub>3</sub> film. However, further investigation is required to evaluate the growth windows of La<sub>2</sub>O<sub>2</sub>CO<sub>3</sub> and SrTiO<sub>3</sub> films.

Each material system has its own growth windows, which define the limited range of thin film deposition. Since the thermal decomposition of the metal-organic precursor is one

of the critical steps in CSD-based thin-film growth, TGA and DTA were introduced to provide detailed insights into the temperature dependence of the decomposition of La<sub>2</sub>O<sub>2</sub>CO<sub>3</sub> solution (Fig. 1). The TGA curve shows three different mass loss stages in the temperature ranges of 100–260 °C, 260–450 °C, and 700–800 °C. In the first stage, the initial melting and dehydration, together with solvent evaporation, start around 100 °C with a mass loss of 25%. In the second stage, mass loss starts around 260 °C and is attributed to nitrate-containing compounds.<sup>22</sup> This leads to a 35% weight reduction and a strong exothermic effect at 398 °C, as shown in the DTA curve (Fig. 1A, dashed line). After 450 °C, the La<sub>2</sub>O<sub>2</sub>CO<sub>3</sub> phase remains stable (orange marking in Fig. 1A), and CO<sub>2</sub> begins to release at 700 °C, causing a 5% mass loss. This leads to a phase transformation to La<sub>2</sub>O<sub>3</sub>, confirmed by an endothermic effect at 803 °C in the DTA curve. The formation of La<sub>2</sub>O<sub>3</sub> phase is undesirable, as it can crystallize in two phases:<sup>23,24</sup> cubic-La<sub>2</sub>O<sub>3</sub> and hexagonal-La<sub>2</sub>O<sub>3</sub>, which can exhibit a large mismatch with the SrTiO<sub>3</sub> thin film. La<sub>2</sub>O<sub>2</sub>CO<sub>3</sub> films, prepared by the CSD method, require loading into the PLD chamber and heating to a specified substrate temperature prior to SrTiO<sub>3</sub> deposition. Therefore, their thermal stability under vacuum conditions was evaluated. As-grown La<sub>2</sub>O<sub>2</sub>CO<sub>3</sub> films were heated to 800 °C and held for 30 minutes in the PLD chamber under vacuum, followed by XRD analysis. The XRD patterns in Fig. 1B reveal a slight reduction in crystallinity, evidenced by peak broadening and a decrease in intensity. No formation of La<sub>2</sub>O<sub>3</sub> phase peaks was observed, indicating phase stability under these conditions. However, the surface roughness for the as-grown La<sub>2</sub>O<sub>2</sub>CO<sub>3</sub> films increases slightly after heating to 800 °C (RMS = 2.01) compared to the unheated films (RSM = 1.13). Therefore, when using the La<sub>2</sub>O<sub>2</sub>CO<sub>3</sub> films as a seed layer for PLD deposition, exposure to high temperatures should be minimized as much as possible.

To determine the appropriate deposition and growth window for the SrTiO<sub>3</sub> thin film, the substrate temperature during PLD deposition was set to 300 °C to form an amorphous film on the La<sub>2</sub>O<sub>2</sub>CO<sub>3</sub>-templated Si(001) substrate, using an SrTiO<sub>3</sub> target as described in the Experimental section. The amorphous thin films were deposited at the lowest chamber pressure of around  $2.1 \times 10^{-5}$  mbar for 5 min and subsequently naturally cooled to room temperature under the same pressure

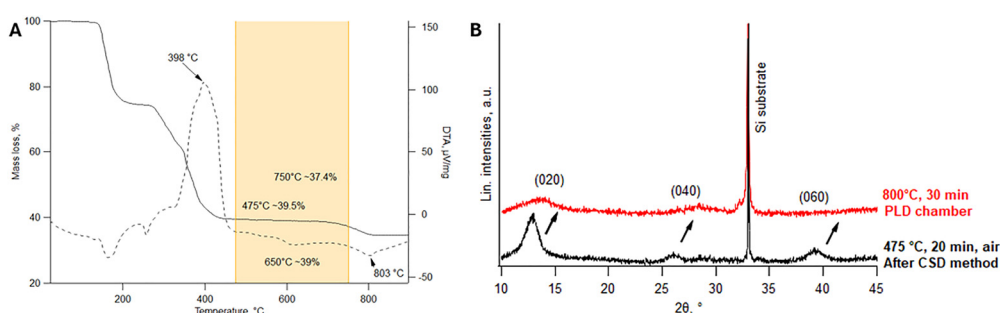


Fig. 1 (A) TGA-DTA record of the La<sub>2</sub>O<sub>2</sub>CO<sub>3</sub> solution with a heating ramp of 10 °C min<sup>-1</sup> under an air atmosphere. (B) Laboratory (Cu K $\alpha$  wavelength) XRD patterns of La<sub>2</sub>O<sub>2</sub>CO<sub>3</sub>-templated Si substrate before (black) and after (red) heating up in the PLD chamber.



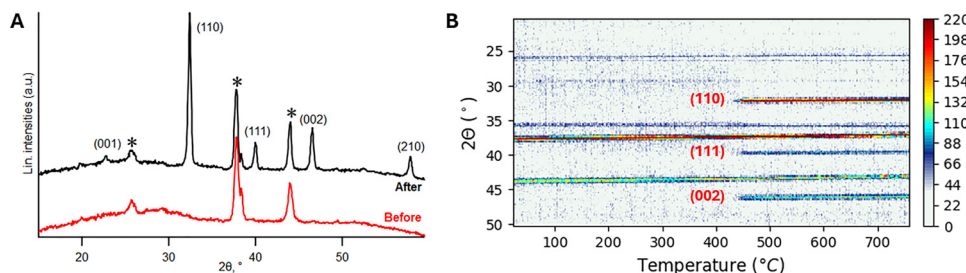


Fig. 2 (A) *Ex situ* XRD laboratory XRD patterns (Cu K $\alpha$  wavelength) of the SrTiO<sub>3</sub> thin film before (red) and after (black) heating experiments. (B) *In situ* XRD scan of the SrTiO<sub>3</sub> film, measured from room temperature to 750 °C. The color scale depicts the intensity of the signal in counts.

before being removed from the PLD chamber. The SrTiO<sub>3</sub> film is amorphous after the deposition, as no peaks of STO are observed on the *ex situ* XRD patterns (Fig. 2A, red line). The crystallization step is necessary to induce the formation of a crystalline SrTiO<sub>3</sub> film. Real-time evolution of the crystallization step from the amorphous phase into polycrystalline SrTiO<sub>3</sub> films is observed by *in situ* XRD (Fig. 2B) scans. At 300 °C, the films are completely amorphous with no identifiable crystalline phases. When heated to 430 °C, several diffraction peaks of the SrTiO<sub>3</sub> cubic phase begin to appear –  $2\theta = 22.783^\circ$  (001),  $32.424^\circ$  (110),  $39.985^\circ$  (111), and  $46.485^\circ$  (002). These observations indicate that polycrystalline SrTiO<sub>3</sub> thin films start to grow from approximately 430 °C under an ambient atmosphere. Further heating to the desired temperature and under a controlled atmosphere will result in a more crystalline SrTiO<sub>3</sub> film with a preferential orientation.

Since the SrTiO<sub>3</sub> deposition window should lie between 475 °C and 750 °C, due to the thermal stability of the La<sub>2</sub>O<sub>2</sub>CO<sub>3</sub> film within this temperature range, we have selected two deposition temperatures of 650 °C and 750 °C. The SrTiO<sub>3</sub> film was deposited using either a one-step method (deposition at the target temperature for 10 min at a specific O<sub>2</sub> pressure of 0.13 mbar) or a two-step method (initial deposition at 300 °C for 1 min at the lowest pressure of  $2.1 \times 10^{-5}$  mbar, followed by a second deposition at the target temperature for 10 min at a specific O<sub>2</sub> pressure of 0.13 mbar). The XRD patterns in Fig. 3A

show that the SrTiO<sub>3</sub> film deposited *via* the two-step method did not crystallize or exhibited poor crystallinity, along with cracks in the film as observed in the planar-view SEM image (Fig. 3C). These cracks indicate that the initial 20 nm thick SrTiO<sub>3</sub> film resulted in high internal stress during crystallization due to volumetric shrinkage and lattice mismatch with the substrate. Reducing the thickness of the amorphous layer could eliminate this crack formation and should be further investigated in a follow-up study. In contrast, the one-step method resulted in good crystallinity, confirmed by diffraction peaks corresponding to (001), (110), and (200) peaks of SrTiO<sub>3</sub>, and a crack-free surface as observed in the planar-view SEM image (Fig. 3B). This indicates that the SrTiO<sub>3</sub> film starts to grow along two orientations simultaneously. At 650 °C, the (110) orientation dominates during deposition, as (110)-oriented grains tend to nucleate first due to an unavoidable mismatch (See Fig. 3A, inset). However, this preferential orientation can be suppressed by increasing the substrate temperature to 750 °C. This behavior is attributed to differences in diffusion energy and the relaxation of internal residual strain along different orientations. A higher substrate temperature promotes the diffusion and relaxation of residual strain within (200)-oriented SrTiO<sub>3</sub> grains, thereby gradually reducing the preferential growth of (110)-oriented grains.<sup>25</sup> However, when the SrTiO<sub>3</sub> film is deposited directly on the Si substrate without the La<sub>2</sub>O<sub>2</sub>CO<sub>3</sub> film, (110)-oriented grains are formed, as shown

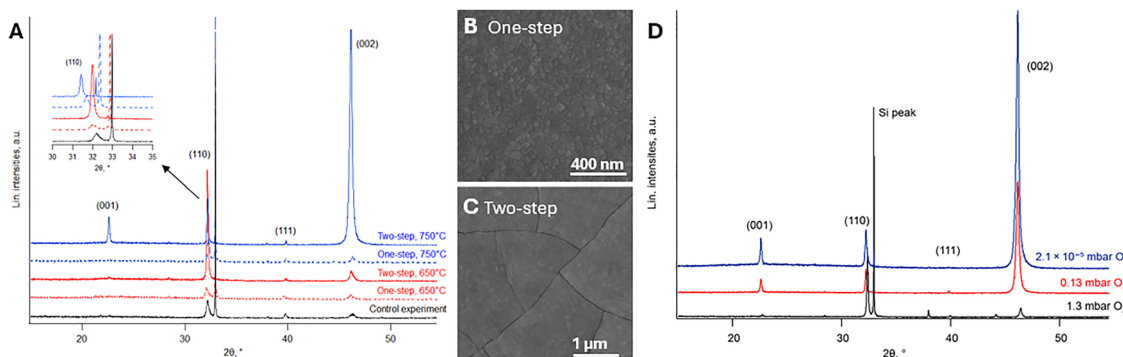


Fig. 3 Laboratory (Cu K $\alpha$  wavelength) XRD scans of the SrTiO<sub>3</sub> films grown on a La<sub>2</sub>O<sub>2</sub>CO<sub>3</sub>-templated Si(100) substrate, deposited at (A) the substrate temperatures of 650 °C and 750 °C *via* the one- or two-step methods. Inset: XRD patterns of the (110) peak are shifted to lower 2θ positions for better visualisation of the differences between the intensities. Planar-view SEM images of the SrTiO<sub>3</sub> film deposited *via* (B) one-step and (C) two-step methods. (D) XRD scans of the SrTiO<sub>3</sub> films deposited *via* a one-step method at 750 °C at different oxygen pressures.



in Fig. 3A (control experiment), due to the larger lattice mismatch and interfacial reactions between the  $\text{SrTiO}_3$  film and the Si substrate. Therefore, the  $\text{La}_2\text{O}_2\text{CO}_3$  film serves as an effective buffer and seed layer, promoting the desired orientation and preventing detrimental interfacial reactions.

As oxygen pressure plays a crucial role in  $\text{SrTiO}_3$  film growth, the films in this study exhibited a bluish color after PLD deposition, which is typically associated with oxygen-deficient  $\text{SrTiO}_3$ .<sup>26</sup> Such oxygen-deficient films are expected to form under low oxygen pressure conditions, as this is generally unavoidable.<sup>27</sup> Therefore, different oxygen pressures (1.3, 0.13, and  $2.1 \times 10^{-5}$  mbar) were introduced to investigate the relative fraction of (110)-oriented grains compared to the (001)-oriented grains. Preferential orientation was evaluated based on the intensities of the (001), (110), (111), and (002) peaks from the XRD patterns (Fig. 3D) using texture coefficients  $\text{TC}(hkl)$ , as defined by the Harris formula.<sup>28</sup> The  $\text{TC}(hkl)$  values of the films grown under 0.13 mbar and  $2.1 \times 10^{-5}$  mbar oxygen pressure exceeded 1 for the (001) and (002) planes, indicating preferential growth along the (001) direction. In contrast, at a higher oxygen pressure of 1.3 mbar, only  $\text{TC}(110)$  was greater than 1, suggesting that higher oxygen pressure promotes growth along the (110) orientation. These results highlight the strong influence of oxygen pressure on the preferential orientation of  $\text{SrTiO}_3$  films during deposition. This effect is further supported by the Lotgering factor (LF), which quantifies the degree of preferred orientation in polycrystalline materials, with higher values indicating stronger texture.<sup>29</sup>  $\text{SrTiO}_3$  film deposited at an oxygen pressure of 0.13 mbar exhibited an LF of 74.96%, indicating a good texture but not complete alignment along the desired orientation. In contrast, deposition under high vacuum conditions ( $2.1 \times 10^{-5}$  mbar) resulted in an even stronger texture, with an LF of 81.22%. This difference in texture can also be explained by the influence of oxygen pressure on the ablated species during PLD, as collisions between the ablated species and oxygen molecules slow down the plume expansion. In high vacuum conditions ( $2.1 \times 10^{-5}$  mbar), the plume expands freely, resulting in higher kinetic energy whereas higher oxygen pressure (1.3 mbar) leads to lower kinetic energy and less crystalline films.<sup>30</sup>

The  $\theta$ - $2\theta$  XRD scans reveal that the  $\text{SrTiO}_3$  film exhibits a preferential out-of-plane orientation along (001) planes. Conversely, synchrotron GIWAXS measurements, performed at shallow incident angles, probe planes that are in the Bragg condition at off-normal orientations. As a result, the 2D GIWAXS patterns for the  $\text{SrTiO}_3$  film are shown in Fig. 4A after remapping of the GIWAXS pattern (missing wedge now shown for clarity). Diffraction spots appear at specific  $\chi$  angles (with  $0^\circ$  as the normal surface direction, *i.e.* out-of-plane and  $90^\circ$  the in-plane direction) for the different planes, proving the preferential orientation of the system. Moreover, the absence of vertical streaks from  $0^\circ$  to  $90^\circ$  confirms that the  $\text{SrTiO}_3$  film does not contain a significant fraction of randomly oriented grains. To assess the in-plane orientation, a pole figure was recorded for the (110) reflection of the  $\text{SrTiO}_3$  film at  $2\theta = 32.44^\circ$  [Cu  $K_\alpha$  wavelength] (Fig. 4B). The presence of a broad and arc-like intensity distribution (partial ring) at  $\chi = 45^\circ$  suggests a degree of alignment. Although this non-uniform ring might initially suggest that there are some preferred in-plane orientations, these features indicate multiple preferred orientations rather than a continuous fibre texture. This suggests that the  $\text{SrTiO}_3$  film shows some degree of ordering, which differs from the expected fibre texture of the  $\text{La}_2\text{O}_2\text{CO}_3$  template film. In conclusion, these observations collectively confirm a preferential out-of-plane orientation along the (001) planes with some preferential in-plane orientation.

The structural quality of the  $\text{SrTiO}_3$  film and its interface with  $\text{La}_2\text{O}_2\text{CO}_3$ -templated Si substrate were examined by high-resolution transmission electron microscopy (HRTEM), as shown in Fig. 5A. The cross-sectional HRTEM images reveal the crystalline  $\text{SrTiO}_3$  film grown on  $\text{La}_2\text{O}_2\text{CO}_3$ -templated Si substrate. The presence of large interference patterns in the HRTEM image (Fig. 5B) corresponds to Moiré fringes.<sup>31</sup> The TEM image at high magnification shows a preferential out-of-plane orientation of the  $\text{SrTiO}_3$  film, which is further confirmed by fast Fourier transform (FFT) analysis (not shown). The variation in the chemical composition across the  $\text{SrTiO}_3$  film was examined using EDX mapping in STEM mode with a high-angle annular dark-field detector. The EDX elemental maps and line profile (Fig. 5C and D) revealed a homogeneous

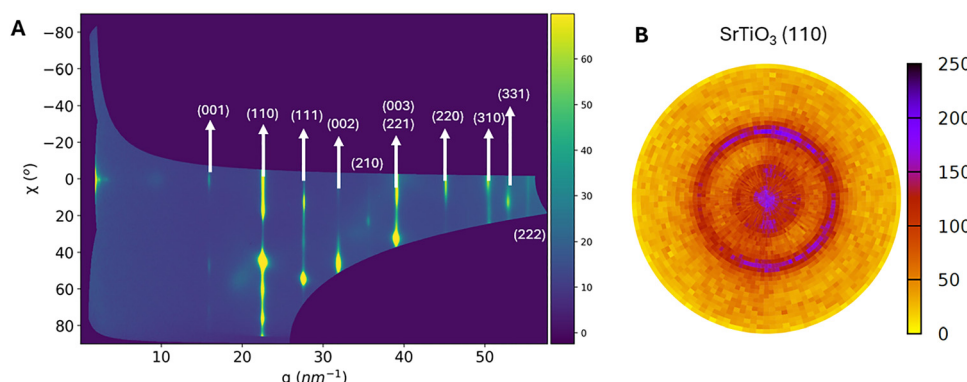


Fig. 4  $\text{SrTiO}_3$  film deposited at  $750^\circ\text{C}$ : (A) the 2D GIWAXS data and (B) the pole figure measurement of the  $\text{SrTiO}_3$  (110) plane measured with a laboratory Cu  $K_\alpha$  source. The color scale depicts the intensity of the signal in counts per second.



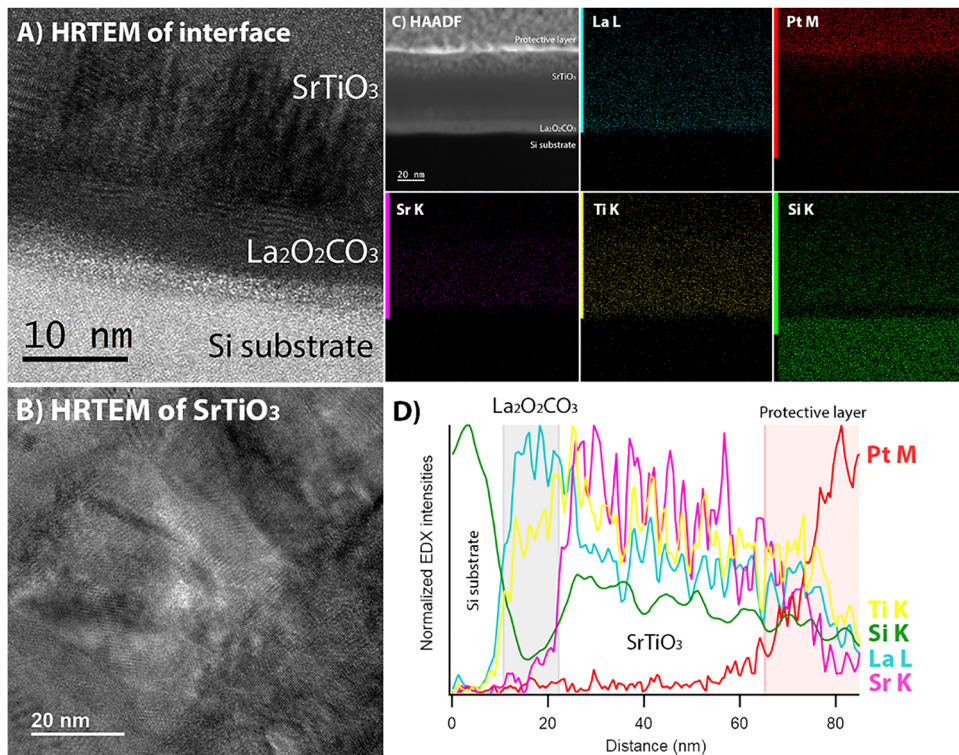


Fig. 5 (A) Cross-sectional HRTEM image, showing the interface between the SrTiO<sub>3</sub> film, La<sub>2</sub>O<sub>2</sub>CO<sub>3</sub> template layer, and the Si substrate. (B) Close-up of the SrTiO<sub>3</sub> film. (C) EDX elemental maps and (D) the cross-sectional cumulated and normalized EDX line profile of the entire stacked layers.

distribution of Sr K and Ti K elements throughout the film, indicating a uniform elemental composition across the SrTiO<sub>3</sub> film. No interfacial reaction was observed, indicating that the La<sub>2</sub>O<sub>2</sub>CO<sub>3</sub> film is also preserved as a barrier layer to prevent the out diffusion of silicon atoms from the substrate to the SrTiO<sub>3</sub> film at high temperature. This observation also confirms that the La<sub>2</sub>O<sub>2</sub>CO<sub>3</sub> film does not decompose under the high kinetic energy of the ablated species during PLD.<sup>32</sup> The SrTiO<sub>3</sub> film thickness is approximately 42 nm after 2 minutes of PLD deposition, corresponding to a growth rate of 0.35 nm per second or 0.035 nm per pulse. Given the SrTiO<sub>3</sub> lattice parameter of 0.3905 nm, this results in an average growth rate of 0.896 monolayer per second.

To demonstrate that the SrTiO<sub>3</sub> film can serve as a texture template or transfer layer for growing a functional perovskite film, a solution-derived BaTiO<sub>3</sub> film was deposited *via* the chemical solution deposition (CSD) method following the procedure in ref. 33. This resulted in a crystalline BaTiO<sub>3</sub> film with preferential (001) orientation, as shown in the XRD patterns (Fig. 6), confirming the effectiveness of the PLD-grown SrTiO<sub>3</sub> film as a template. However, for further implementation in targeted applications where orientation control and crystalline quality are crucial, these templates and functional films should be further investigated in follow-up studies. Such studies should include time-resolved data during the PLD deposition to monitor SrTiO<sub>3</sub> film growth *via* *in situ* reflection high-energy electron diffraction (RHEED) and explore various PLD parameters.<sup>30,34</sup> This combination of solution-based

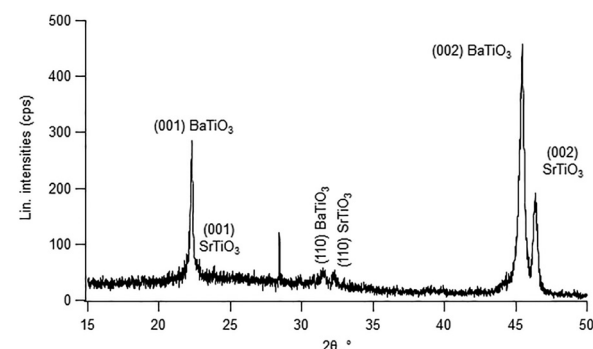


Fig. 6 XRD patterns of the solution-derived BaTiO<sub>3</sub> film deposited on a PLD-grown SrTiO<sub>3</sub> film on the La<sub>2</sub>O<sub>2</sub>CO<sub>3</sub>-coated Si substrate.

deposition with PLD can reduce fabrication costs and enhance high-throughput processing efficiency compared to vacuum-based techniques such as MBE. This highlights its suitability for large-area and wafer-scale fabrication and scalable integration on Si-based platforms.

In summary, this work demonstrates that the La<sub>2</sub>O<sub>2</sub>CO<sub>3</sub> film can serve as both a seed and barrier layer, providing an effective template for the integration of high-quality and textured SrTiO<sub>3</sub> thin films on silicon substrates. Analysis of the growth windows of both materials is essential before PLD, as the stability of the solution-derived buffer layer plays a critical role. Careful control of PLD parameters, especially substrate temperature and

oxygen pressure, is required to achieve preferential but not exclusive (001) out-of-plane orientation of crystalline  $\text{SrTiO}_3$  thin films. One-step PLD at 750 °C under low oxygen or vacuum pressure produced crack-free films with excellent crystallinity and uniform composition, confirmed *via* XRD and TEM. This confirms the potential of  $\text{La}_2\text{O}_2\text{CO}_3$ -assisted growth strategies for integrating functional perovskite oxide films on silicon-based platforms.

## Conflicts of interest

There are no conflicts to declare.

## Data availability

The data underlying this study is available in Zenodo at <https://doi.org/10.5281/zenodo.12759437>, and can be accessed freely.

## Acknowledgements

H. R. acknowledges support and funding as a postdoctoral fellow for fundamental research from the Research Foundation-Flanders (FWO) under grant number 1273621N. GIWAXS patterns were measured at the ALBA synchrotron facility with the collaboration of the ALBA staff.

## References

- 1 E. Mikheev, B. D. Hoskins, D. B. Strukov and S. Stemmer, Resistive switching and its suppression in Pt/Nb:  $\text{SrTiO}_3$  junctions, *Nat. Commun.*, 2014, **5**, 3990, DOI: [10.1038/ncomms4990](https://doi.org/10.1038/ncomms4990).
- 2 K. S. Randhawa, Advanced ceramics in energy storage applications: Batteries to hydrogen energy, *J. Energy Storage*, 2024, **98**, 113122, DOI: [10.1016/j.est.2024.113122](https://doi.org/10.1016/j.est.2024.113122).
- 3 A. Ulrich, K. Brahim, A. Boelen, M. Debaets, A. Khalil, C. Sun, Y. Huang, S. S. Saseendran, M. Baryshnikova, P. Favia, T. Nuytten, S. Sergeant, K. Van Gasse, B. Kuyken, K. De Greve, C. Merckling and C. Haffner, Engineering high Pockels coefficients in thin-film strontium titanate for cryogenic quantum electro-optic applications, *Science*, 2025, **390**(6771), 390–393, DOI: [10.1126/science.adx3741](https://doi.org/10.1126/science.adx3741).
- 4 J. Haeni, P. Irvin, W. Chang, R. Uecker, P. Reiche, Y. Li, S. Choudhury, W. Tian, M. Hawley and B. Craig, Room-temperature ferroelectricity in strained  $\text{SrTiO}_3$ , *Nature*, 2004, **430**, 758–761, DOI: [10.1038/nature02773](https://doi.org/10.1038/nature02773).
- 5 S. Zhang, J. Deliyore-Ramírez, S. Deng, B. Nair, D. Pesquera, Q. Jing, M. E. Vickers, S. Crossley, M. Ghidini and G. G. Guzmán-Verri, *et al.*, Highly reversible extrinsic electrocaloric effects over a wide temperature range in epitaxially strained  $\text{SrTiO}_3$  films, *Nat. Mater.*, 2024, **23**, 639–647, DOI: [10.1038/s41563-024-01831-1](https://doi.org/10.1038/s41563-024-01831-1).
- 6 G. Niu, S. Yin, G. Saint-Girons, B. Gautier, P. Lecoeur, V. Pillard, G. Hollinger and B. Vilquin, Epitaxy of  $\text{BaTiO}_3$  thin film on Si (001) using a  $\text{SrTiO}_3$  buffer layer for non-volatile memory application, *Microelectron. Eng.*, 2011, **88**, 1232–1235, DOI: [10.1016/j.mee.2011.03.028](https://doi.org/10.1016/j.mee.2011.03.028).
- 7 Z. Wang, H. P. Nair, G. C. Correa, J. Jeong, K. Lee, E. S. Kim, C. S. Lee, H. J. Lim, D. A. Muller and D. G. Schlom, Epitaxial integration and properties of  $\text{SrRuO}_3$  on silicon, *APL Mater.*, 2018, **6**, 086101, DOI: [10.1063/1.5041940](https://doi.org/10.1063/1.5041940).
- 8 O. Nakagawara, M. Kobayashi, Y. Yoshino, Y. Katayama, H. Tabata and T. Kawai, Effects of buffer layers in epitaxial growth of  $\text{SrTiO}_3$  thin film on Si (100), *J. Appl. Phys.*, 1995, **78**, 7226–7230, DOI: [10.1063/1.360433](https://doi.org/10.1063/1.360433).
- 9 M. Spreitzer, D. Klement, T. Parkelj Potočnik, U. Trstenjak, Z. Jovanović, M. D. Nguyen, H. Yuan, J. E. ten Elshof, E. Houwman and G. Koster, *et al.*, Epitaxial ferroelectric oxides on silicon with perspectives for future device applications, *APL Mater.*, 2021, **9**, 040701, DOI: [10.1063/5.0039161](https://doi.org/10.1063/5.0039161).
- 10 G. Delhaye, C. Merckling, M. El-Kazzi, G. Saint-Girons, M. Gendry, Y. Robach, G. Hollinger, L. Largeau and G. Patriarche, Structural properties of epitaxial  $\text{SrTiO}_3$  thin films grown by molecular beam epitaxy on Si (001), *J. Appl. Phys.*, 2006, **100**, 124109, DOI: [10.1063/1.2407273](https://doi.org/10.1063/1.2407273).
- 11 M. Spreitzer, R. Egoavil, J. Verbeeck, D. H. Blank and G. Rijnders, Pulsed laser deposition of  $\text{SrTiO}_3$  on a H-terminated Si substrate, *J. Mater. Chem. C*, 2013, **1**, 5216–5222, DOI: [10.1039/C3TC30913D](https://doi.org/10.1039/C3TC30913D).
- 12 V. Vaithyanathan, J. Lettieri, W. Tian, A. Sharan, A. Vasudevarao, Y. Li, A. Kochhar, H. Ma, J. Levy and P. Zschack, c-axis oriented epitaxial  $\text{BaTiO}_3$  films on (001) Si, *J. Appl. Phys.*, 2006, **100**, 024108, DOI: [10.1063/1.2203208](https://doi.org/10.1063/1.2203208).
- 13 L. Goncharova, D. Starodub, E. Garfunkel, T. Gustafsson, V. Vaithyanathan, J. Lettieri and D. Schlom, Interface structure and thermal stability of epitaxial  $\text{SrTiO}_3$  thin films on Si (001), *J. Appl. Phys.*, 2006, **100**, 014912, DOI: [10.1063/1.2206710](https://doi.org/10.1063/1.2206710).
- 14 Z. Wang, B. Goodge, D. Baek, M. Zachman, X. Huang, X. Bai, C. Brooks, H. Paik, A. Mei and J. Brock, Epitaxial  $\text{SrTiO}_3$  film on silicon with narrow rocking curve despite huge defect density, *Phys. Rev. Mater.*, 2019, **3**, 073403, DOI: [10.1103/PhysRevMaterials.3.073403](https://doi.org/10.1103/PhysRevMaterials.3.073403).
- 15 P. Dinari, C. Chandra, J. Suwardy, S. Mustofa and Y. Darma,  $\text{SrTiO}_3$  Thin Films Deposition Using Pulsed Laser Deposition Technique, *Adv. Mater. Res.*, 2013, **789**, 72–75, DOI: [10.4028/www.scientific.net/AMR.789.72](https://doi.org/10.4028/www.scientific.net/AMR.789.72).
- 16 M. D. Nguyen, H. Yuan, E. P. Houwman, M. Dekkers, G. Koster, J. E. Ten Elshof and G. Rijnders, Highly oriented growth of piezoelectric thin films on silicon using two-dimensional nanosheets as growth template layer, *ACS Appl. Mater. Interfaces*, 2016, **8**, 31120–31127, DOI: [10.1021/acsami.6b09470](https://doi.org/10.1021/acsami.6b09470).
- 17 M. Nijland, S. Thomas, M. A. Smithers, N. Banerjee, D. H. Blank, G. Rijnders, J. Xia, G. Koster and J. E. ten Elshof, Epitaxy on demand, *Adv. Funct. Mater.*, 2015, **25**, 5140–5148, DOI: [10.1002/adfm.201501483](https://doi.org/10.1002/adfm.201501483).
- 18 D. H. Blank, M. Dekkers and G. Rijnders, Pulsed laser deposition in Twente: from research tool towards industrial deposition, *J. Phys. D: Appl. Phys.*, 2013, **47**, 034006, DOI: [10.1088/0022-3727/47/3/034006](https://doi.org/10.1088/0022-3727/47/3/034006).



19 E. Picavet, H. Rijckaert, E. Solano, O. Bikondoa, E. G. Fernandez, P. Paturi, L. Van Bossele, H. Vrielinck, J. Beeckman and K. De Buysser, The self out-of-plane oriented  $\text{La}_2\text{O}_2\text{CO}_3$  film: an integration tool for fiber textured ferroelectric thin films, *J. Mater. Chem. C*, 2023, **11**, 7705–7713, DOI: [10.1039/D3TC01046E](https://doi.org/10.1039/D3TC01046E).

20 J. George, P. Smet, J. Boterman, V. Bliznuk, W. Woestenborghs, D. Van Thourhout, K. Neyts and J. Beeckman, Lanthanide-assisted Deposition of Strongly Electro-optic PZT Thin Films on Silicon: Toward Integrated Active Nanophotonic Devices, *ACS Appl. Mater. Interfaces*, 2015, **7**, 13350–13359, DOI: [10.1021/acsmami.5b01781](https://doi.org/10.1021/acsmami.5b01781).

21 H. Rijckaert, Preparation of the S/TEM Lamella of Commercial  $\text{REBa}_2\text{Cu}_3\text{O}_{7-x}$  Coated Conductors by FIB, *IEEE Trans. Appl. Supercond.*, 2024, **34**(7), DOI: [10.1109/TASC.2024.3438690](https://doi.org/10.1109/TASC.2024.3438690).

22 H. Guerreiro, P. Melnikov, I. Arkhangelsky, L. de Oliveira, G. Wandekoken and V. do Nascimento, Thermal decomposition of lanthanum nitrate hexahydrate  $\text{La}(\text{NO}_3)_3 \cdot 6\text{H}_2\text{O}$ , *Int. J. Dev. Res.*, 2021, **11**, 43318–43321, DOI: [10.37118/ijdr.20799.01.2021](https://doi.org/10.37118/ijdr.20799.01.2021).

23 C. Yang, H. Fan, Y. Xi, S. Qiu and Y. Fu, Anomalous phase formation during annealing of  $\text{La}_2\text{O}_3$  thin films deposited by ion beam assisted electron beam evaporation, *Thin Solid Films*, 2009, **517**, 1677–1680, DOI: [10.1016/j.tsf.2008.09.069](https://doi.org/10.1016/j.tsf.2008.09.069).

24 A. Yadav, A. Lokhande, R. Pujari, J. Kim and C. Lokhande, The synthesis of multifunctional porous honey comb-like  $\text{La}_2\text{O}_3$  thin film for supercapacitor and gas sensor applications, *J. Colloid Interface Sci.*, 2016, **484**, 51–59, DOI: [10.1016/j.jcis.2016.08.056](https://doi.org/10.1016/j.jcis.2016.08.056).

25 J. Ye, S. Mou, R. Zhu, L. Liu and Y. Li, Orientation competition growth and mechanism of  $\text{SrTiO}_3$  film on  $\text{CeO}_2$  layer, *Vacuum*, 2021, **194**, 110626, DOI: [10.1016/j.vacuum.2021.110626](https://doi.org/10.1016/j.vacuum.2021.110626).

26 C. W. Schneider, M. Döbeli, C. Richter and T. Lippert, Oxygen diffusion in oxide thin films grown on  $\text{SrTiO}_3$ , *Phys. Rev. Mater.*, 2019, **3**, 123401, DOI: [10.1103/PhysRevMaterials.3.123401](https://doi.org/10.1103/PhysRevMaterials.3.123401).

27 H. N. Lee, S. S. Ambrose Seo, W. S. Choi and C. M. Rouleau, Growth control of oxygen stoichiometry in homoepitaxial  $\text{SrTiO}_3$  films by pulsed laser epitaxy in high vacuum, *Sci. Rep.*, 2016, **6**, 19941, DOI: [10.1038/srep19941](https://doi.org/10.1038/srep19941).

28 M. Bannur, K. Maddani, S. Mathad and P. Patil, Structural and Optical Properties of (110) Plane Textured  $\text{SnO}_2:\text{Zn}$  Thin Films, *Int. J. Self-Propag. High-Temp. Synth.*, 2019, **28**, 34–38, DOI: [10.3103/S1061386219010035](https://doi.org/10.3103/S1061386219010035).

29 J. L. Jones, E. B. Slamovich and K. J. Bowman, Critical evaluation of the Lotgering degree of orientation texture indicator, *J. Mater. Res.*, 2004, **19**, 3414–3422, DOI: [10.1557/JMR.2004.0440](https://doi.org/10.1557/JMR.2004.0440).

30 N. A. Shepelin, Z. P. Tehrani, N. Ohannessian, C. W. Schneider, D. Pergolesi and T. Lippert, A practical guide to pulsed laser deposition, *Chem. Soc. Rev.*, 2023, **52**, 2294–2321, DOI: [10.1039/D2CS00938B](https://doi.org/10.1039/D2CS00938B).

31 X. Ke, M. Zhang, K. Zhao and D. Su, Moiré fringe method via scanning transmission electron microscopy, *Small Methods*, 2022, **6**, 2101040, DOI: [10.1002/smtd.202101040](https://doi.org/10.1002/smtd.202101040).

32 M. J. Aziz, Film growth mechanisms in pulsed laser deposition, *Appl. Phys. A: Mater. Sci. Process.*, 2008, **93**, 579–587, DOI: [10.1007/s00339-008-4696-7](https://doi.org/10.1007/s00339-008-4696-7).

33 E. Picavet, E. Lievens, K. De Geest, H. Rijckaert, E. G. Fernandez, O. Bikondoa, E. Solano, P. Paturi, N. Singh and T. Pannier, Integration Of Solution-Processed  $\text{BaTiO}_3$  Thin Films with High Pockels Coefficient on Photonic Platforms, *Adv. Funct. Mater.*, 2024, **34**, 2470214, DOI: [10.1002/adfm.202403024](https://doi.org/10.1002/adfm.202403024).

34 M. M. Aye, E. Rivasto, M. Z. Khan, H. Rijckaert, E. Salojärvi, C. Haalisto, E. Mäkilä, H. Palonen, H. Huhtinen and I. Van Driessche, Control of the nanosized defect network in superconducting thin films by target grain size, *Sci. Rep.*, 2021, **11**, 6010, DOI: [10.1038/s41598-021-85304-4](https://doi.org/10.1038/s41598-021-85304-4).

